Quinine Copolymer Reporters Promote Efficient Intracellular DNA Delivery and Illuminate Protein-Induced Unpackaging Mechanism

Classification: Physical Sciences

Authors: Craig Van Bruggen[a,1], David Punihaole[a,1,2], Allison R. Keith[b], Andrew J. Schmitz[a], Jakub Tolar[b], Renee R. Frontiera[a,3], and Theresa M. Reineke[a,3]

[a]Department of Chemistry, University of Minnesota, Minneapolis, Minnesota 55455, United States, [b]Department of Pediatrics, Stem Cell Institute, University of Minnesota Medical School, Minneapolis, Minnesota 55455, United States

Abstract

Polymeric vehicles that efficiently package and controllably release nucleic acids enable the development of safer and more efficacious strategies in genetic and polynucleotide therapies. Developing delivery platforms that endogenously monitor the molecular interactions, which facilitate binding and release of nucleic acids in cells, would aid in the rational design of more effective vectors for clinical applications. Here, we report the facile synthesis of a copolymer containing quinine and 2-hydroxyethyl acrylate that effectively compacts plasmid DNA (pDNA) through electrostatic binding and intercalation. This polymer system poly(quinine-*co*-HEA) packages pDNA and shows exceptional cellular internalization, transgene expression, and low cytotoxicity compared to commercial controls for several human cell lines, including HeLa, HEK 293T, K562, and keratinocytes (N/TERTs). Using quinine as an endogenous reporter for pDNA intercalation, Raman imaging revealed that proteins inside cells facilitate the unpackaging of polymer-DNA complexes (polyplexes) and the release of their cargo. Our work showcases the

ability of quinine copolymer reporter (QCRs) to not only facilitate effective gene delivery, but also enable diagnostic monitoring of polymer-pDNA binding interactions on the molecular scale via Raman imaging. The use of Raman chemical imaging, novel to the field of gene delivery, yields unprecedented insight into the unpackaging behavior of polyplexes in cells and provides a new methodology to assess and design more efficient delivery vehicles for gene-based therapies.

Significance

Polymer-based vehicles that controllably deliver therapeutic nucleic acids to cells show great potential to develop safe and effective gene therapies. Realizing this potential, however, is limited by the lack of understanding of how polymers unpackage their cargo. We developed a quinine-containing polymer that shows exceptional gene delivery activity. A key aspect of this platform is that the quinine serves as a reporter for DNA binding using Raman spectroscopy. This allows us to track cargo release inside the cell using Raman chemical imaging. We find that proteins dominate the unpackaging of DNA encapsulated by these quinine polymers inside cells. This trackable delivery system should be broadly applicable to study nucleic acid delivery mechanisms, as well as be used for clinical therapy applications.

Author contributions: C.V.B., D.P., R.R.F., and T.M.R designed research; C.V.B., D.P., and A.R.K performed research; C.V.B., D.P., and A.J.S analyzed data; J.T., R.R.F., and T.M.R provided new reagents/analytic tools; and C.V.B., D.P., A.R.K., R.R.F, and T.M.R wrote the paper.

Conflict of interest statement: A provisional U.S. Provisional Application (62/536,427) on this work has been filed.

This article is a PNAS Direct Submission.

[1]Authors contributed equally to this work.

[2]Present Address: Department of Chemistry, University of Vermont, 82 University Place, Burlington, Vermont 05405, United States

[3]To whom correspondence should be addressed. Emails: treineke@umn.edu, rrf@umn.edu.

Introduction

Transport of exogenous genetic material into cells in an efficient and nontoxic manner is universal and essential for life science and medical research. Developing effective delivery vehicles is a major limiting factor for the clinical translation of nucleic acid-based gene therapies (e.g., DNA, RNA, CRISPR/Cas9) (**1-3**). The most commonly used delivery vectors in clinical trials are recombinantly engineered viruses that often suffer from translational limitations, such as long manufacturing times, high cost, small cargo capacity, immunogenicity, and limited shelf-life (**4, 5**). As such, progress in the gene and cell therapy field has been limited despite recent breakthroughs with costly FDA-approved treatments (**6, 7**). Chemically synthesized vehicles such as polymer- and lipid-based systems serve as attractive alternatives due to their high-throughput and inexpensive production, ability to be chemically tuned, capacity to encapsulate a large breadth of cargo sizes (oligonucleotides to large plasmids), and accommodation of multiple dosing regimens (**8-10**). Despite these attractive features, however, the delivery efficiency of most polymeric vehicles is lower than viruses, and they can exhibit cytotoxicity (**11**).

Polymer delivery vehicles package their nucleic acid cargo into nanoparticle complexes called polyplexes. Polyplexes perform many dynamic functions during their biological transport pathway, including cargo stabilization en route to the tissue of interest, cell surface contact, endocytosis and intracellular transport, as well as localization and unpackaging at the site-of-action within the cytoplasm or nucleus (**12**). The successful delivery and expression of a plasmid after this process is known as transfection. One contributing factor for the lower transfection efficiencies of polymer delivery systems lies in the fact that polyplexes must be stable outside of the cell (to prevent premature unpackaging) yet enable destabilization once inside the cell to release their nucleic acid cargo. However, for most polymer-based delivery systems, there is relatively little

understanding of the factors and mechanisms that govern the release of nucleic acids from polyplexes within the cell – a necessary step in efficient transgene delivery. It has long been speculated that polyplex unpackaging in cells is facilitated by the interaction of cytosolic proteins and nucleic acids with polymers (**13-15**). However, direct structural evidence for protein-induced unpackaging inside cells is lacking, and it is unclear how or where in the cell they interact with polymers to facilitate cargo release (**12**, **15**). Understanding these and other factors that dictate intracellular unpackaging is necessary to control the fine balance between polyplex stability from extracellular transport, unwanted tissue interactions that can lead to toxicity, and intracellular cargo release to promote gene regulatory efficacy.

Alongside several synthetic methods (**16-19**), the administration of the antimalarial drug chloroquine during transfection has been commonly employed to promote intracellular pDNA unpackaging (**20**). In addition to promoting endosomal escape (**21-23**), chloroquine has been shown to facilitate unpackaging of pDNA by competitive binding (**24**, **25**). Like chloroquine, the structurally similar Cinchona alkaloid, quinine, can bind DNA through both electrostatic interactions with the phosphate backbone and intercalation through π-stacking interactions with nucleobases (**26**, **27**). Therefore, incorporating quinine into a polymer would enable robust DNA binding and polyplex stabilization via multiple binding mechanisms, which minimizes the overall charge density of the polymer necessary to compact DNA. Reducing the polymer's charge density reduces its toxicity profile (**9**), while allowing for increased incorporation of an uncharged comonomer, like 2-hydroxyethyl acrylate (HEA), that serves a complimentary function such as promoting unpackaging. In addition, quinine has well-characterized spectroscopic properties and is a natural product produced in large scale. Thus, facile methods to incorporate quinine into a polymer could yield an inexpensive and effective gene delivery agent with endogenous

spectroscopic properties for diagnostic polyplex imaging. Currently, there is no precedent for incorporating quinine into polymeric delivery vehicles to enhance transfection.

Efforts to rationally design polymers that can more efficiently release nucleic acids at their site-of-action have been hindered by the difficulty of quantitatively tracking the intracellular transport and cargo unpackaging of polyplexes in cells. Most experimental methods to study polyplex unpackaging involves fluorescently labelling nucleic acids and/or their polymeric carriers with large organic probes and monitoring the colocalization of their respective signals (**28**, **29**). The major drawback to this method, however, is that the carrier and cargo must separately diffuse roughly 200 nm, beyond the resolving power of the microscope, in order to detect the dissociation of polyplexes. This distance is two orders of magnitude larger than the spatial scales relevant to polymer binding to nucleic acids, which means that most physiologically-relevant unpackaging dynamics in polyplexes are missed using conventional microscopy methods. Although Förster resonance energy transfer (FRET) has aided in understanding polyplex unpackaging (**30**), accurate quantification of dissociation using fluorescence-based techniques is complicated by spectral cross-talk, photobleaching, phototoxicity, and inconsistent labeling efficiency. In addition, the necessity of using bulky organic fluorophores or quantum dots may perturb the biological mechanisms and unpackaging dynamics of polyplexes (**23**, **31**).

Raman imaging is a powerful tool for characterizing intracellular polyplex unpackaging without the need for utilizing bulky labels. In recent years, Raman microscopy has been increasingly used in biological applications, including monitoring cell changes during drug delivery (**32**), as well as the distribution of lipids (**33**, **34**) and metabolites (**35**) that cannot be easily monitored with fluorescence-based techniques. A major advantage of Raman spectroscopy is that it monitors vibrations that are intrinsically sensitive to the structure and interactions of molecules

6

(**36-41**). We recently showed, for example, that the Raman bands of quinine show characteristic frequency shifts that report on its electrostatic, hydrogen bonding, and π-stacking interactions, which can be used to monitor its intercalation with DNA (**26**). Despite this, the rich chemical information encoded in Raman spectra has surprisingly not been exploited in imaging applications to probe how macromolecules dynamically interact with their local physiochemical environment *in situ*.

Herein, we hypothesize that direct incorporation of quinine into polymeric delivery vehicles could: 1) improve the transfection efficiencies of polyplexes via enhanced binding and release mechanisms; and 2) enable direct monitoring of cargo unpackaging in cells by exploiting its unique fluorescence and Raman-active spectroscopic properties. To accomplish this, we copolymerized quinine with HEA in a one-step free-radical polymerization reaction and demonstrate that this copolymer is exceptionally efficient at delivering plasmids to several human cell types, including keratinocytes, for which suitable transfection methods are limited. We find that poly(quinine-*co*-HEA) exhibits strong binding to pDNA in polyplexes due to quinine's ability to intercalate between nucleotides. By exploiting quinine's spectral sensitivity, Raman imaging directly reveals that proteins facilitate the deintercalation of quinine from pDNA and the unpackaging of polyplexes inside cells (Fig. 1). Our work highlights the tremendous potential of quinine copolymer reporters (QCRs) as an efficient, trackable delivery platform and showcases the unique ability of Raman microscopy to quantitatively probe the molecular interactions *in situ* that facilitate polyplex internalization, cellular transport, and unpackaging.
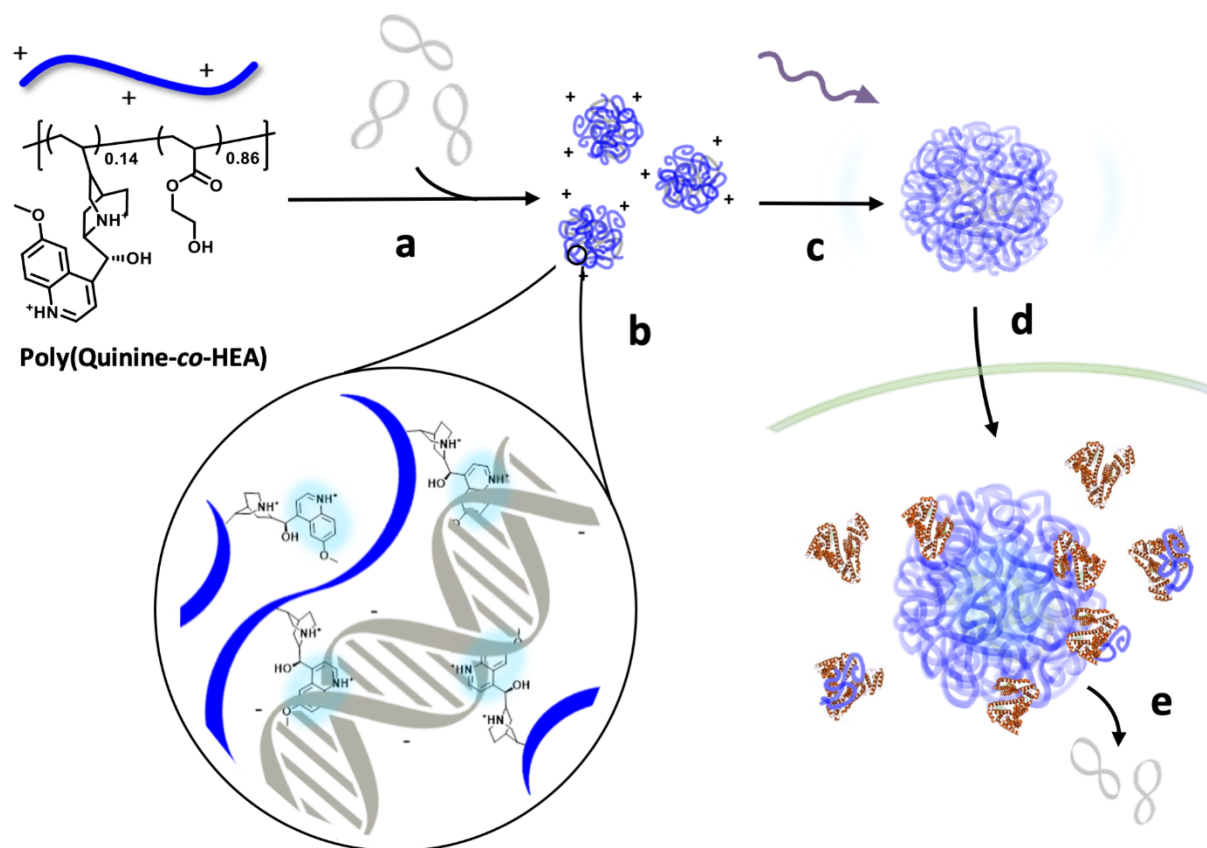
Fig. 1. Mechanisms underlying unique plasmid binding and release mechanisms of quinine copolymer reporters (QCRs). (*A*) Poly(quinine-*co*-HEA) self-assembles with plasmid DNA at low pH (3-4) to form polyplexes and compacts the plasmid (*B*) via electrostatic forces as well as binding via π-stacking interactions. (*C*) Dilution in cell media causes aggregation of the polyplexes, which promotes sedimentation of plasmid to the cell surface. The fluorescent particles (λ_{ex} = 350 nm, λ_{em} = 450 nm) are uptaken (*D*), in part, by macropinocytosis. (*E*) Raman imaging is used to quantify release of pDNA by exposure to intracellular proteins.

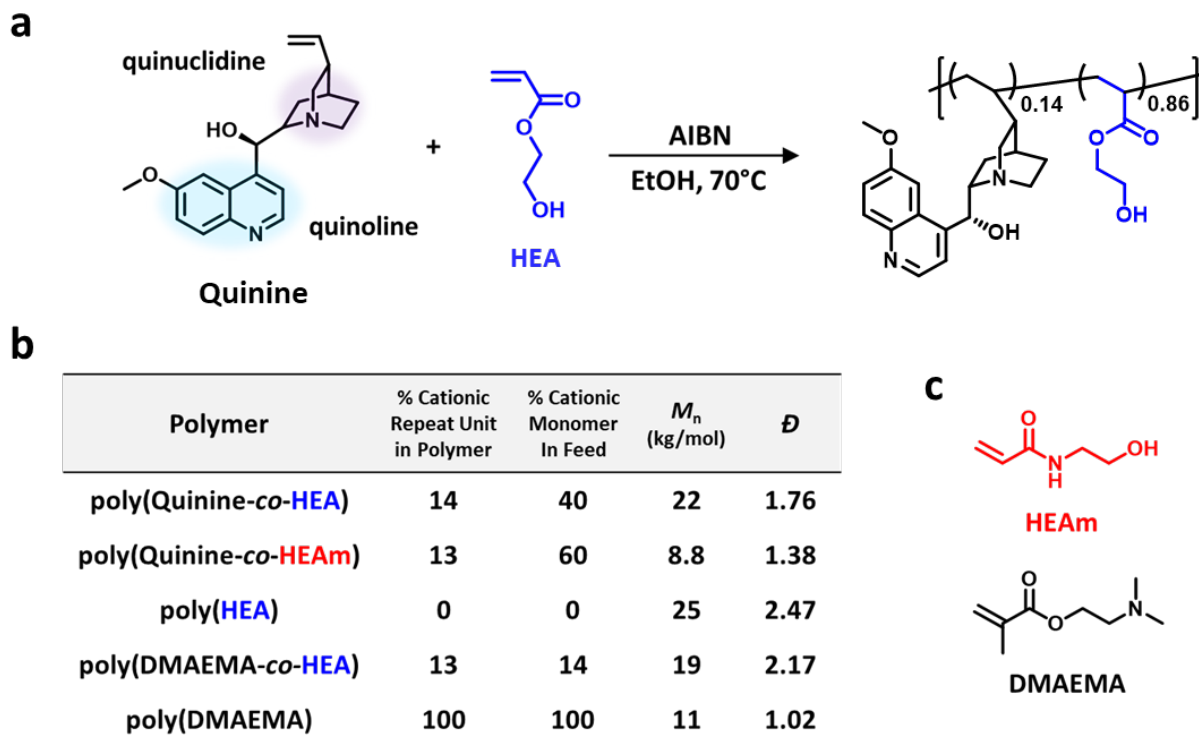**Results and Discussion**

QCR and Control Polymer Synthesis.

Polymer	% Cationic Repeat Unit in Polymer	% Cationic Monomer In Feed	M_n (kg/mol)	Đ
poly(Quinine-*co*-HEA)	14	40	22	1.76
poly(Quinine-*co*-HEAm)	13	60	8.8	1.38
poly(HEA)	0	0	25	2.47
poly(DMAEMA-*co*-HEA)	13	14	19	2.17
poly(DMAEMA)	100	100	11	1.02

Fig. 2. Synthesis and characterization of QCRs and controls. (*A*) Free-radical copolymerization scheme used in this study to incorporate quinine, consisting of a bicyclic quinuclidine head group and fluorescent quinoline ring (λ_{ex} = 350 nm, λ_{em} = 450 nm), into copolymers with comonomers such as 2-(hydroxyethyl) acrylate (HEA; blue). (*B*) Structural properties of polymers used in biological studies as determined by ^{1}H NMR and SEC. (*C*) Quinine was copolymerized with various acrylamides including 2-(hydroxyethyl) acrylamide (HEAm), and HEA was copolymerized with canonical cationic comonomers such as 2-(dimethylamino)ethyl methacrylate (DMAEMA).

9

We sought a facile, one-pot reaction to incorporate quinine into a polymer using inexpensive, commercially available starting materials. Quinine contains several functional handles that enable it to be incorporated into a polymeric scaffold, including its secondary hydroxyl (**42-44**), tertiary amine (**45-47**) and α-olefin groups (**48-52**) (Fig. 2*A*). We first pursued development of reaction conditions that would promote the direct incorporation of quinine into a polymeric backbone via radical propagation of its α-olefin group. While degradative chain transfer and steric hindrance of the bulky quinuclidine ring were needed challenges to overcome (**52-54**), the advantage to a direct approach is three-fold: 1) quinine can be used directly in a copolymerization reaction to enable a rapid, inexpensive, and scalable production method; 2) the quinuclidine amine can be protonated aiding electrostatic interactions with DNA; and 3) the quinoline ring is distal from the backbone, which allows these polymer pendant groups to effectively intercalate into DNA without steric hindrance and allow reporting of binding and release via microscopic and spectroscopic methods.

We found that while quinine cannot be directly homopolymerized (**51**), quinine was active to copolymerization with more reactive comonomers, and we fully characterized the reactivity ratios with several comonomers to enable tuning of chemical composition. We copolymerized quinine with several hydrophilic acrylate- and acrylamide-based comonomers that have not been copolymerized with quinine previously including HEA, 2-(hydroxyethyl) acrylamide (HEAm), acrylamide (Am), N,N-dimethyl acrylamide (DMAm), and N-isopropylacrylamide (NIPAm) (Fig. 2*B*,*C* and *SI Appendix*, Fig. S1). The quinine copolymers we created contained up to 17% quinine by molarity, as determined by ^{1}H-NMR (*SI Appendix*, Fig. S3-7), and polymers were obtained that ranged between 9–22 kDa in molar mass (Fig. 2*C*, *SI Appendix*, Fig. S8 and Table S1). The reactivity ratios of quinine with comonomers HEA, HEAm, and Am were monitored via ^{1}H NMR

10

(*SI Appendix*, Fig. S9). The reactivity ratios for all three comonomers were found to be $r_1 < 0.2$ and $r_2 > 10$. These values indicate that quinine is statistically incorporated within the polymer chains as isolated units spaced by hydrophilic repeat units. These hydrophilic comonomers acted as spacer units between quinine repeat units, which improves the solubility, reduces charge density, and toxicity of cationic polymers, as shown in polyethyleneimine (PEI) derivatives and carbohydrate-based polycations (**9**, **55-57**). The architecture was also further confirmed via a combination of size exclusion chromatography (SEC), differential refractive index, UV-Vis, and static light scattering (SLS) analysis showing that quinine was equally distributed along each copolymer chain (not a mixture of two homopolymers) and that all polymer chains contained quinine (*SI Appendix*, Fig. S8). The molar masses, dispersities, and architectures of the synthesized copolymers are comparable to other effective polymeric delivery agents (**58-60**). Overall, this direct approach to successfully propagate quinine via copolymerization is simple, inexpensive, reproducible, and readily scalable, making it amenable for numerous fundamental and translational research endeavors.
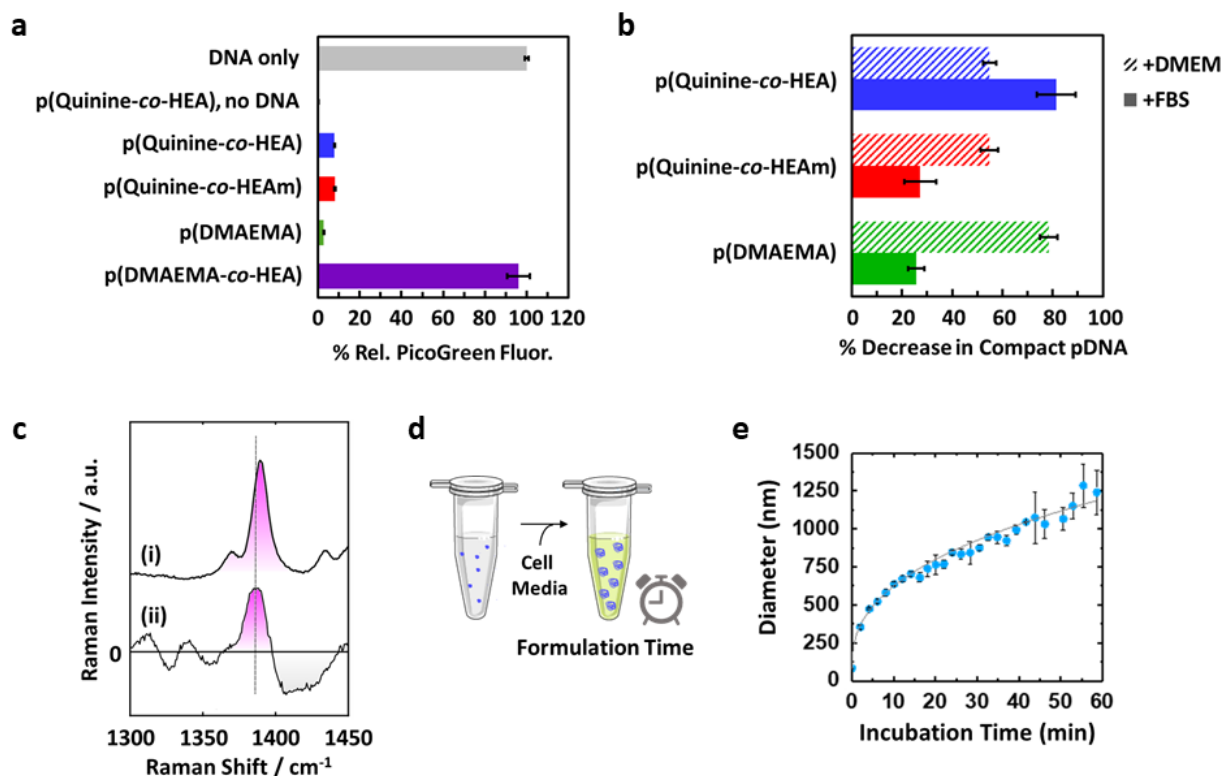
Quinine facilitates enhanced binding to DNA in polyplexes.

Fig. 3. Characterization of QCR-DNA binding. (*A*) Dye exclusion assay monitors pDNA compaction in polyplexes (N/P = 6) formed in acidic aqueous media (pH 3-4). The fluorescence of PicoGreen intercalation in polyplexes is normalized to the fluorescence from free pDNA. (*B*) The polyplex solution in (*A*) is diluted first in cell media (DMEM) followed by addition of fetal bovine serum (FBS, 10% v/v). The change in relative PicoGreen fluorescence upon sequential addition of solutions is used to calculate the percent decrease in compact pDNA between steps. (*C*) (i) Raman spectrum of unbound poly(quinine-*co*-HEA) polymer under acidic solution conditions and (ii) difference spectrum highlighting the spectral shift that occurs in the quinoline ring mode of poly(quinine-*co*-HEA) due to DNA intercalation. The difference in the quinoline ring mode frequency (3 cm^{-1}) between intercalated and deintercalated quinine can be used to monitor poly(quinine-*co*-HEA) polyplex unpackaging. (*D*) Schematic of polyplex aggregation in

serum-free DMEM prior to exposure to cells (defined as formulation time). (*E*) Plot showing the hydrodynamic diameter of poly(quinine-*co*-HEA) polyplexes (N/P = 8) over time after addition of serum-free DMEM. Data for (a), (b), and (e) represented as the mean ± SD (n = 3).

Our previous work shows that monomeric quinine interacts with DNA electrostatically via the quinuclidine moiety, as well as through intercalation via the quinoline ring (**26**). We hypothesized that the quinine copolymers would efficiently bind and compact pDNA and form self-assembled polyplexes in solution via both binding modes, allowing for protection against degradation and efficient cellular delivery. Electrophoretic mobility shift assays demonstrate that all the quinine copolymer variants were able to bind pDNA (*SI Appendix*, Fig. S11) at a range of formulation N/P ratios as low as N/P = 0.5, which is defined as the molar ratio of quinuclidine amines (N) to DNA phosphate groups (P). Dynamic light scattering (DLS) showed that quinine copolymers self-assemble with plasmids in solution to form positively charged polyplexes between roughly 80 - 200 nm in hydrodynamic diameter (d_h) (*SI Appendix*, Fig. S12-13). Like many transfection reagents, we found that poly(quinine-*co*-HEA) polyplexes aggregated upon dilution of serum-free cell media due to de-protonation at neutral pH (*SI Appendix*, Fig. S10, S12-13) (**60**, **61**). Interestingly, we discovered that the aggregation of poly(quinine-*co*-HEA) polyplexes upon addition of serum-free DMEM could be controlled as the mean polyplex size (d_h) increases monotonically to approximately 1 µm within 60 min (Fig. 3*E*). Indeed, polyplex aggregation has been shown to promote transfection by increasing sedimentation of DNA, which concentrates the polyplexes at the cell surface and increases the amount DNA that is internalized (**62-65**). This control in particle size can be used to directly tune and improve biological efficacy (see below).

Analogous copolymer controls were created that replaced quinine with canonical amines, such as 2-(dimethylamino)ethyl methacrylate (DMAEMA) (**57, 65**) (Fig. 2*A* and *SI Appendix*, Fig. S2) to remove the intercalation ability for comparison. Using a dye exclusion assay, we found that when quinine was replaced with DMAEMA in a HEA copolymer, the ability of the copolymer to compact pDNA was completely inhibited (Fig. 2*A* and *SI Appendix*, Fig. S14). The QCRs maintained more pDNA compaction upon dilution in serum-free media compared to polyplexes formed with the DMAEMA homopolymer (Fig. 2*B* and *SI Appendix*, Fig. S14-15). This result shows that quinine has exceptional DNA binding and compaction properties compared to canonical amine-containing monomers such as DMAEMA, which is likely due to the dual binding mechanism of electrostatics and intercalation.

The mechanism underlying the exceptional compaction of pDNA by quinine in poly(quinine-*co*-HEA) was further investigated using Raman spectroscopy. We previously proved that the quinoline ring symmetric stretching mode (referred to as the quinoline ring mode henceforth) quantitatively reports on the local interactions of quinine with its chemical environment (**26**). In the case of monomeric quinine, the quinoline ring mode characteristically upshifts in frequency upon deintercalation from DNA due to the loss of π-stacking interactions with nucleobases (*SI Appendix*, Table S3). To examine the binding of quinine to DNA in the copolymers, we measured the Raman spectra of poly(quinine-*co*-HEA) polyplexes under similar pH conditions as the DLS and dye exclusion assays. To highlight the changes that occur due to binding, the spectral contributions of free pDNA and poly(quinine-*co*-HEA) polymers not bound to DNA were subtracted (*SI Appendix*, Fig. S26). The resulting difference spectrum (Fig. 3*C* (ii)) shows a prominent positive feature at 1386 cm^{-1} that derives from the quinoline ring mode and is downshifted 3 cm^{-1} from the same band in the unbound polymer solution (Fig. 3C(i) and *SI*

Appendix, Table S3). This frequency shift therefore quantitates the intercalation of quinine into pDNA and can be used as a spectroscopic marker to monitor the degree of polyplex packaging and unpackaging. Taken together, the dye exclusion and Raman spectroscopic results indicate that quinine binds to DNA through both electrostatic interactions with the phosphate backbone and π-stacking with the nucleobases, which contributes to the overall stability of the polyplex formulations. Collectively, the confluence of these characteristics confers copolymers containing quinine with considerable compaction capabilities compared to canonical cationic amine-containing constituents.

Optimization of Delivery Performance

We first screened our library of QCRs for their ability to deliver plasmids encoding for either luciferase or ZsGreen (a green fluorescent protein) to HeLa cells. We determined transfection efficiency by either measuring the total output of protein by a culture (luciferase) or by measuring the percentage of cells positive for ZsGreen. Interestingly, when quinine was copolymerized with an acrylamide, such as HEAm, Am, NIPAm, or DMAm, the resulting polyplexes were unable to achieve transgene expression (*SI Appendix*, Fig. S16). Poly(quinine-*co*-HEA), however, showed exemplary transfection efficiencies with both reporter plasmids, and provided a 58% increase in ZsGreen expression efficiency as compared to the gold-standard commercial control Lipofectamine 2000 (*SI Appendix*, Fig. S16). Upon finding a hit comonomer type, we determined the optimal molar ratio of quinine needed for transfection using a luciferase-based transfection screen with a small library of poly(quinine-*co*-HEA) copolymers containing between 3-17% quinine by molarity (*SI Appendix*, Table S2). We found that the variant containing 14% quinine by molarity yielded at least three-fold higher gene expression compared to the other variants (*SI Appendix*, Fig. S16).
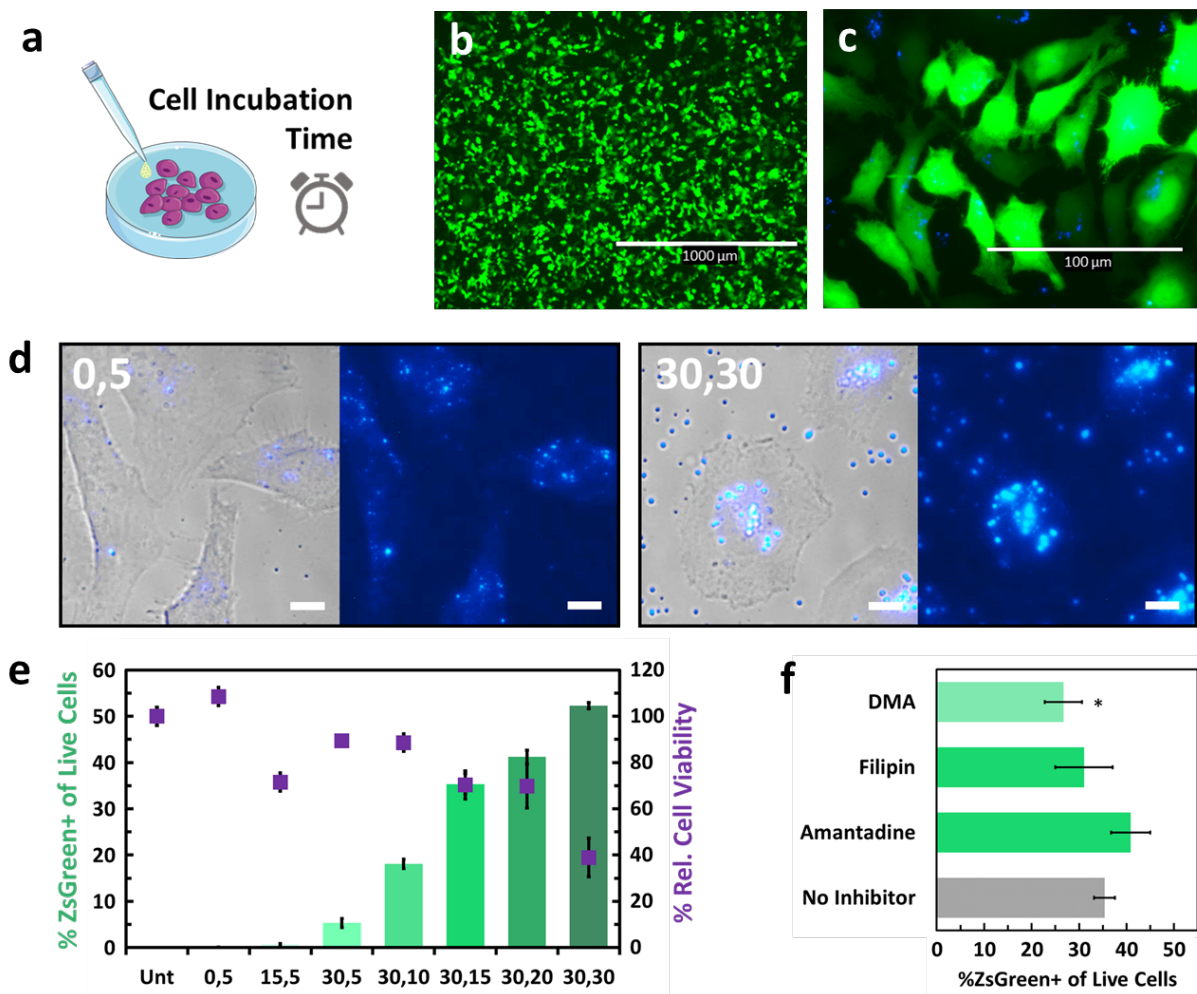
Fig. 4. Fluorescence of intracellular polyplexes containing quinine and size-dependent activity.

(*A*) After the "formulation time" (Fig. 3*D*) to achieve the desired mean particle diameter, the poly(quinine-*co*-HEA) polyplexes were incubated with HeLa cells for a defined time (defined as "cell incubation time"). (*B,C*) Images of fixed HeLa cells 48 hrs post-transfection with pZsGreen and poly(quinine-*co*-HEA) (N/P = 8) at (*B*) 4× magnification with poly(quinine-*co*-HEA) (blue) and (*C*) 40× magnification. (*D*) Images of HeLa cells fixed 6 hrs post-transfection with poly(quinine-*co*-HEA) at various formulation and cell incubation times. The sample names [i,ii]

are derived from (i) formulation time (Fig. 3*D*) and (ii) cell incubation time (Fig. 4*A*). Left image in each pair is an overlay of transmission and polymer (blue), while the right image is of polymer only. Scale bar = 10 μm. (*E*) Bar graph showing the percent transfection efficiency of live cells (as determined by flow cytometry) and relative cell viability (as determined by CCK-8 cell counting kit) 48 hrs post-transfection. (*F*) HeLa cells transfected with the conditions shown for sample [30,15] in (*E*) were incubated with endocytosis inhibitors. Incubation with DMA (macropinocytosis inhibitor) gives a statistically significant reduction in transfection indicating macropinocytosis contributes to successful transfection of aggregated polyplexes. Data for (*E*) and (*F*) represented as the mean ± SD (n = 3); *$P < 0.05$.

Focusing on optimizing biological performance with the variant of poly(quinine-*co*-HEA) containing 14% quinine, we looked to our previous discovery of polyplex size control (Fig. 3*C,D*). By adding the polyplex solution to cells at specific periods along the aggregation time course, we could control the average diameter of polyplexes that the cells were exposed to during the transfection experiments and correlate its efficiency in transfection to particle size (Fig. 4*A-C*). Using quinine's endogenous fluorescence (*SI Appendix,* Fig. S18), we used fluorescence microscopy to measure and track particles of various sizes in the intracellular space (Fig. 4*C-D* and *SI Appendix,* Fig. S19-20). The calculated mean diameters of the internalized particles in the widefield images were similar in hydrodynamic diameters measured via DLS for the corresponding formulation time (*SI Appendix,* Fig. S21*A*). In addition, microscopy verified that increased cell incubation times led to an increase in internalized particles (*SI Appendix,* Fig. S21*B*). We measured the transfection efficiency with ZsGreen for each timeframe and observed that both particle size and number of internalized particles positively correlated to ZsGreen expression

efficiency as well as cytotoxicity (Fig. 4*E*, see *SI Appendix* for details). Indeed, a fine balance between transfection performance and cytotoxicity in this system exists and can be tailored by controlling the incubation periods that affect both polyplex size and number of particles internalized by cells. The tight control allows for differential transgene delivery to target cell populations without introducing variability into cargo load.

To understand why large particles enabled higher transfection efficiencies, we investigated which internalization mechanism was the greatest contributor to transgene expression of large particles by inhibiting different modes of endocytosis with small molecule inhibitors. We probed clathrin-mediated endocytosis, caveolae-dependent endocytosis, and macropinocytosis with the inhibitors amantadine, fillipin III, and 5-(N,N-dimethyl)amiloride hydrochloride (DMA), respectively (Fig. 4*F*). A significant decrease in transfection efficiency for DMA-treated cells suggests that macropinocytosis contributes as an internalization route of poly(quinine-*co*-HEA) polyplexes that leads to gene expression. Aggregation of the polyplexes may allow the polyplexes to bypass unproductive endocytic routes limited to smaller size capacities (**66**, **67**).

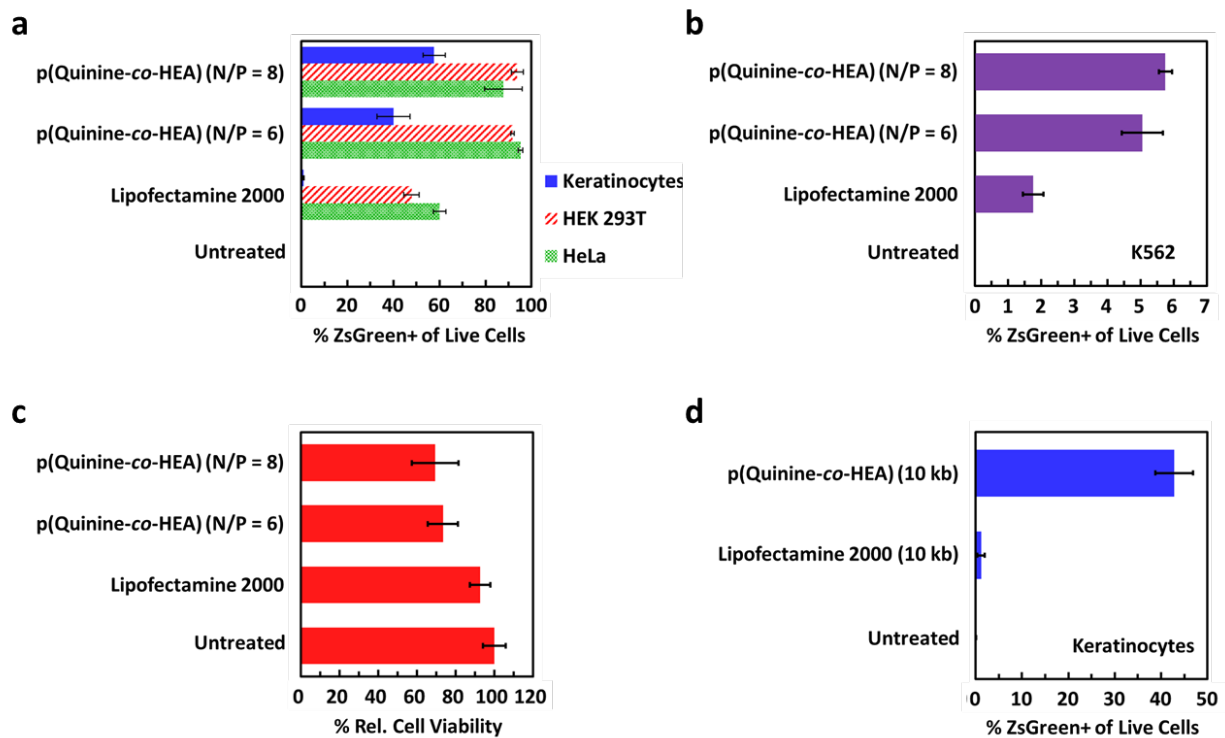**Efficient Transfection in Multiple Cell Types.**

Fig. 5. QCR variant of poly(quinine-*co*-HEA) containing 14% quinine efficiently transfects a variety of cell types. (*A,B*) The transfection efficiency in the delivery of pZsGreen (4.7 kb plasmid) to adherent cell lines (HeLa and HEK 293T), keratinocytes, and suspension cell line K562 was improved significantly by using poly(quinine-*co*-HEA) compared to Lipofectamine 2000 as - determined by flow cytometry 48 hours post transfection. (*C*) The cell viability of HEK 293T cells was determined 48 hours post transfection via CCK-8 assay. (*D*) Efficient transfection of keratinocytes using a large plasmid (10 kb, pZsGreen) was maintained using poly(quinine-*co*-HEA). Data (*A-D*) represented as the mean ± SD (n = 3).

Efficient transgene delivery is a challenge in many cell-focused investigations, particularly in experiments involving primary or transfection-resistant cell types important for research and cell therapy development. To explore the utility of the QCR poly(quinine-*co*-HEA) variant containing 14% quinine in overcoming this barrier in other cell types, we identified the N/P ratios that balanced efficient delivery of a ZsGreen fluorescent reporter plasmid with minimal cytotoxic effects. Excellent delivery performance with poly(quinine-*co*-HEA) was achieved with transfection-amenable adherent cell types such as HEK 293T (Fig. 5*A* and *SI Appendix,* Fig. S22*A*) and HeLa (Fig. 4*B-F*, Fig. 5*A*). In HEK 293T cells, we observed excellent transfection efficiency ($\geq$ 92% ZsGreen+) at N/P $\geq$ 6 (Fig. 5*A* and *SI Appendix*, Fig. S22*A*), which is the minimum N/P ratio needed for full compaction of DNA (*SI Appendix*, Fig. S12, 14). In comparison, Lipofectamine 2000 demonstrated a lower transfection efficiency (48%) but higher relative cell viability (93%, Fig. 5*C* and *SI Appendix,* Fig. S22*B*). We next assessed its application in a suspension cell type (lymphoblast line K562) via increasing complex dose to account for decreased surface area in suspension cells. We found that poly(quinine-*co*-HEA) (N/P = 6 and 8) transfection efficiencies (5.1 and 5.8%, respectively) in K562 cells exhibited a 3-fold improvement over Lipofectamine 2000 (1.8%) (Fig. 5*B* and *SI Appendix,* Fig. S23). Indeed, these results support previous work that sedimentation of polyplexes onto the cell surface (Fig. 4) aids optimal transgene delivery.

We next tested the efficacy of poly(quinine-*co*-HEA)-mediated gene delivery in keratinocytes, a transfection-resistant cell type that is a vital component in the upper layer of the skin and important to modeling and treatment of genetic skin disorders such as epidermolysis bullosa. Gene editing of keratinocytes, performed for autologous transplants to repair diseased and

damaged skin, have primarily relied on viral vectors due to their high transfection efficiency (**68-70**). Viral vectors, however, are severely restricted in cargo capacity (i.e. adeno associated viruses are limited to ~4.7 kb of cargo), which limits their ability to deliver large therapeutic proteins or gene editing machinery. In addition, common nonviral alternatives have proven to be inefficient in transfecting keratinocytes. We performed a ZsGreen transfection in this cell type (Fig. 5*A*) with Lipofectamine 2000 and found poor transfection efficiencies (<1% ZsGreen+) that corroborated the results seen in literature (0-4% transfection efficiency) (**71-73**). Efficient transfection could be achieved, however, with poly(quinine-*co*-HEA) (58% ZsGreen+ for N/P = 8). Interestingly, we also performed transfection with a plasmid double in size (10 kb, Fig. 5*D*), which yielded 43% ZsGreen+ cells after transfection with poly(quinine-*co*-HEA) as compared to only 1.2% for Lipofectamine 2000. These results demonstrate the versatility of this vehicle for diverse and transfection-resistant cell types as well as large gene payload sizes relevant to numerous challenging diseases (i.e., dystrophin for muscular dystrophy treatment and collagen for genetic skin diseases).

HEA facilitates decompaction of DNA in the presence of protein.

We hypothesized that the interplay between polymer binding to DNA and release of the cargo plays an important role in the excellent performance of the QCR poly(quinine-*co*-HEA). It is known that, for *in vivo* applications, protein binding can cause premature unpackaging of polyplexes (**61**). Consistent with this, we observed that titrating increasing amounts of FBS into poly(quinine-*co*-HEA) polyplex solutions prior to transfection leads to a dose-dependent decrease in transgene expression (*SI Appendix,* Fig. S24). We recognized, however, that for important *ex vivo* cell therapy applications serum-free media can be used during transfection. Thus, exposure to protein can be limited to the intracellular space (after endocytosis), which could be an important factor to stimulate the unpackaging of polyplexes. To examine the influence of protein binding, we added fetal bovine serum (FBS) to polyplex solutions diluted in cell media and monitored their unpackaging using a dye exclusion assay (Fig. 3*B*). Upon addition of FBS, the pDNA bound by poly(quinine-*co*-HEA) decomplexed by over 3-fold more than poly(DMAEMA). When the acrylate in the copolymer (HEA) was replaced with an acrylamide analogue (HEAm), this dramatic decomplexation by FBS was eliminated. This result indicates that the acrylate in poly(quinine-*co*-HEA) facilitates polymer binding to protein, which also leads to pDNA unpackaging. This finding is supported by DLS (see *SI Appendix,* Fig. S12*B* for details) and by work from Zhao et al. who observed higher levels of serum binding to the HEA polymer brushes compared to the acrylamide analogue due to decreased surface hydration (**74-76**). This investigation supports the hypothesis that while quinine is needed for efficient binding of pDNA outside the cell, the HEA comonomer facilitates pDNA release from polyplexes upon exposure to intracellular protein.

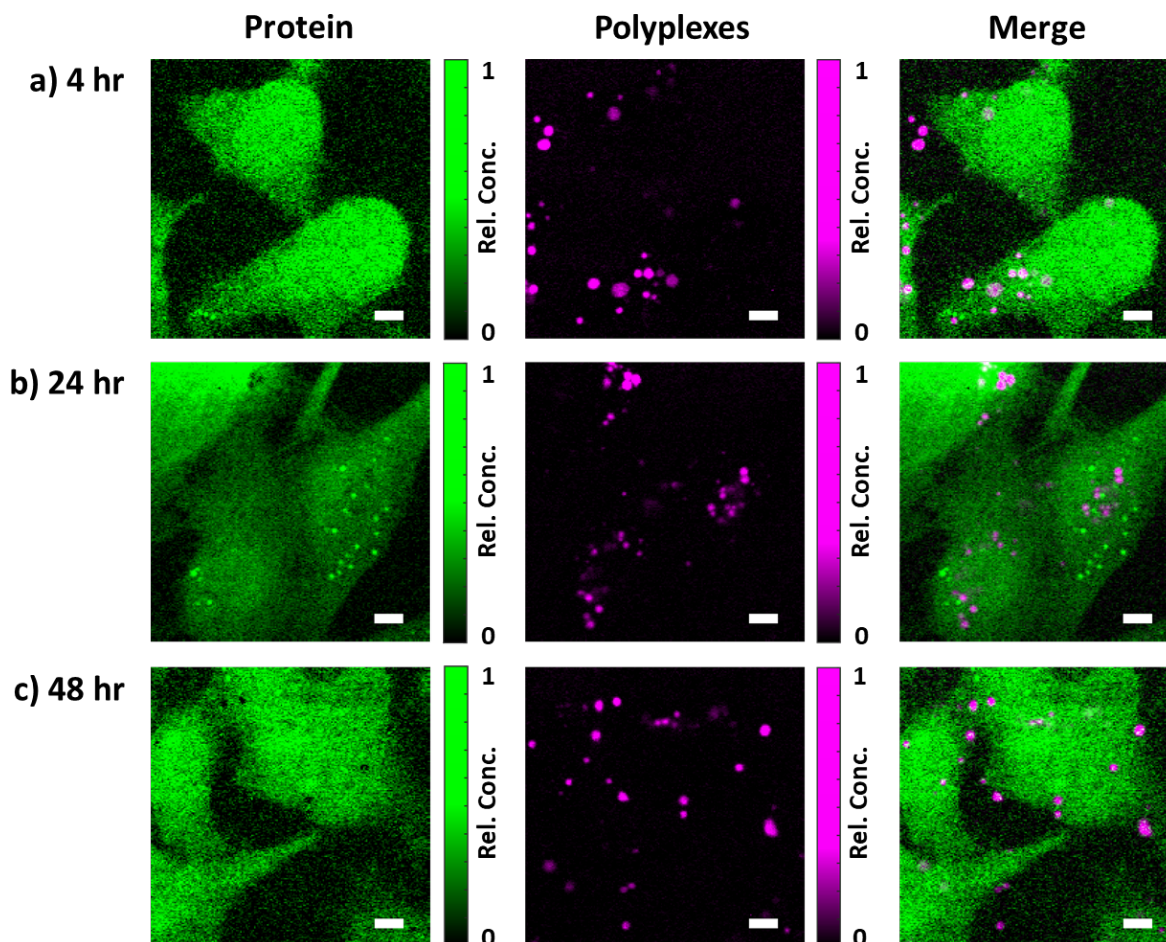**Raman imaging verifies protein-induced unpackaging within cells**

Fig. 6. Representative Raman images of HeLa cells and QCR polyplex particles after (*A*) 4 hrs, (*B*) 24 hrs, and (*C*) 48 hrs post-transfection. Cells (green) were visualized using the integrated intensity of the protein Amide I band (1660 cm^{-1}), while polyplex particles (magenta) were visualized by the quinoline ring mode of quinine (1369 cm^{-1}). The overlay of these images shows the presence of both intracellular and extracellular particles at all timepoints. Scale bars = 5 μm.

The utility of the inherent reporting properties of poly(quinine-*co*-HEA) are highlighted via confocal Raman microscopy tracking experiments that quantify quinine deintercalation and further support the hypothesis that proteins facilitate polyplex unpackaging inside cells. Using Raman microscopy to monitor quinine-pDNA binding within poly(quinine-*co*-HEA) polyplexes, we were able to correlate the presence of protein within the polyplexes to pDNA unpackaging during the transfection process. HeLa cells were treated with poly(quinine-*co*-HEA) polyplexes and fixed for Raman hyperspectral imaging 4, 24, and 48 hours after transfection. Each pixel in these images contained a Raman spectrum that roughly spanned a region from 900 - 1800 cm^{-1} (Fig. 6). These hyperspectral images were analyzed using principal component analysis (PCA) in order to identify spectroscopic signatures of polyplex dissociation (*SI Appendix*, Fig. S27-28). All of the images that were analyzed contained at least one principal component (PC) whose loading vector showed the quinoline ring mode at 1369 cm^{-1} (Fig. 7*A,B*), indicative of the quinine moieties in poly(quinine-*co*-HEA) intercalating into DNA. However, in the 48-hour post-transfection images shown in Fig. 6c, we identified PCs whose loading vectors showed quinoline ring modes that were upshifted to 1372 cm^{-1} (Fig. 7C,D), which signaled the deintercalation of quinine from pDNA. The PC score maps in Fig. 7*A,C* were used to determine the percent deintercalation of quinine moieties (*SI Appendix,* Fig. S29), which allowed for the degree of polyplex unpackaging to be quantified (Fig. 7*F*). On average, we observed that roughly 10 – 30% of quinine moieties were deintercalated from DNA in the polyplexes shown in Fig. 6*C*. However, our analysis allowed us to observe unpackaging heterogeneities not only between, but also within, the particles themselves. For example, while many particles exhibited a fairly uniform unpackaging landscape, some particles showed most of their unpackaging on the exterior, giving rise to ring-shaped patterns (inset of Fig.

7*F*). The presence of these ring-shaped patterns suggests that the unpackaging of the DNA suffuses from the outside-in, akin to surface erosion.
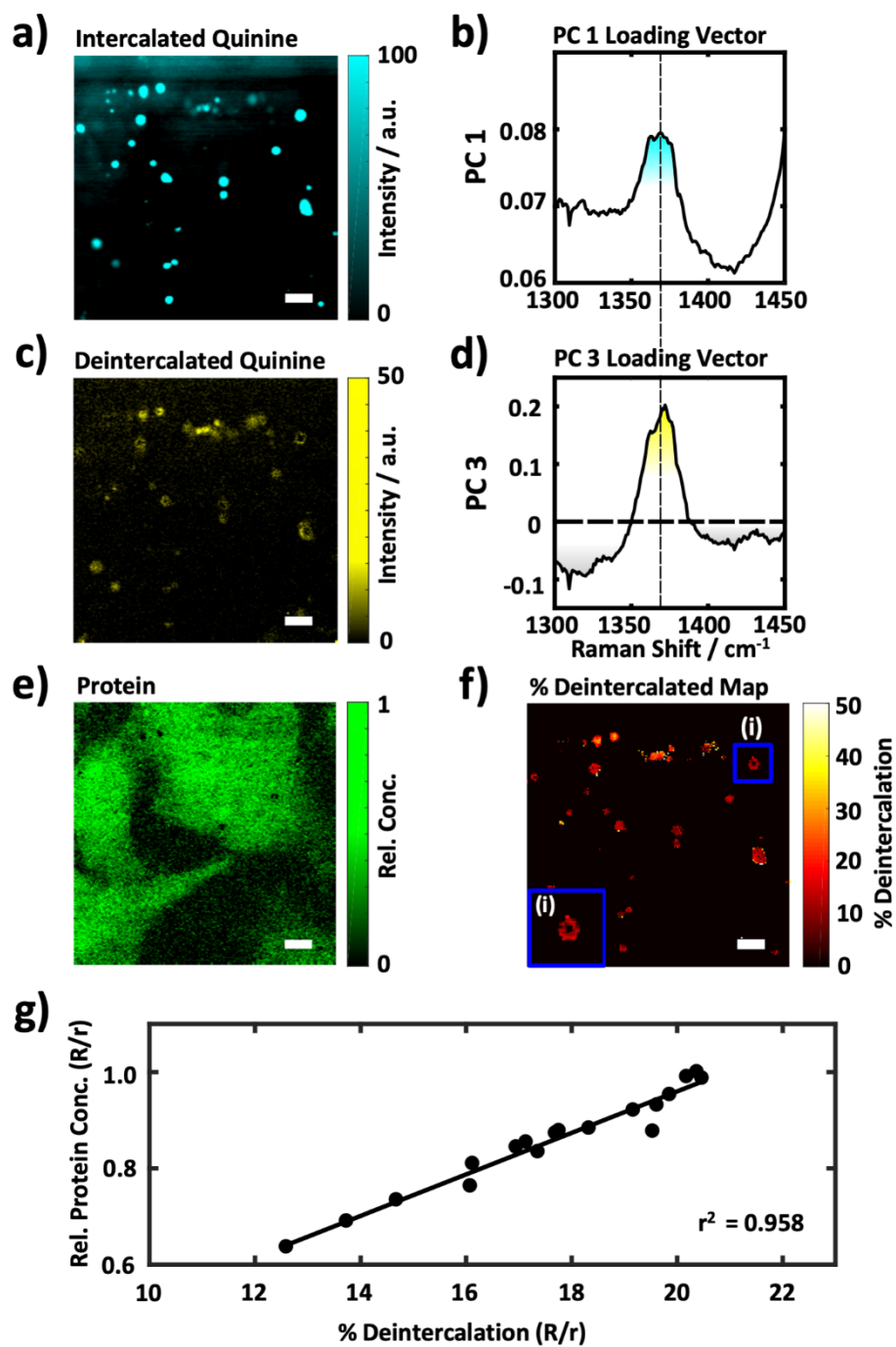
Fig. 7. Results from PCA of Raman hyperspectral images for HeLa cells 48 hrs post-transfection. (*A*) PC 1 score map showing the relative concentration of quinine moieties in poly(quinine-co-HEA) polyplexes that are DNA-intercalated. (*B*) PC 1 loading vector showing the 1369 cm^{-1} quinoline ring stretching mode spectral signature indicative of quinine-DNA intercalation. (*C*) PC 3 score map showing the relative concentration of quinine moieties in polyplexes that are deintercalated from pDNA. (*D*) PC 3 loading vector showing the 1372 cm^{-1} quinoline ring stretching mode indicative of quinine deintercalation. (*E*) Raman image showing the relative concentration of protein distributed in the cells. The PC score maps shown in (*A,C*) were used to determine (*F*) the percent deintercalation for every pixel of the polyplex particles. The inset shown in panel (*F*) shows a magnified region containing a polyplex with a ring-shaped unpackaging behavior. (*G*) Correlates the percent deintercalation with respect to the relative concentration of protein as a function of the normalized distance (R/r) from the centroids of polyplex particles inside cells (see *SI Appendix* for details). Scale bars = 5 μm.

In order for the particles to undergo unpackaging from the surface inwards, there is likely some component in the intracellular milieu that is facilitating unpackaging. It is unlikely that the unpackaging of the polyplexes is facilitated by hydrolysis of the HEA pendant groups since HEA is stable within the intracellular pH range encountered by polyplexes (*SI Appendix,* Fig. S25). Instead, our dye exclusion results (Fig. 3*B*) indicate that intracellular proteins are likely causing polyplex unpackaging. If this were the case, we would expect to observe a correlation between the concentration of protein and pDNA deintercalation in the polyplex particles. To investigate this, we calculated the radially averaged cross sections of all the individual particles to quantify the distribution of poly(quinine-*co*-HEA), pDNA unpackaging, and proteins as a function of distance

inside the polyplexes (*SI Appendix,* Fig. S30). The radial cross section of the relative polymer concentration decreased monotonically from the centroid of the particles. In contrast, the radial cross sections corresponding to the deintercalation of poly(quinine-*co*-HEA) from pDNA and the relative protein concentration do not follow this monotonic behavior, but instead mirror each other. In fact, as indicated in Fig. 7*G*, the relative concentration of protein colocalized with polyplex particles is strongly correlated (r^2 = 0.958) with the percentage of poly(quinine-*co*-HEA) quinine moieties that are deintercalated from the DNA cargo.

This remarkable linear correlation indicates that proteins dominate the unpackaging of the poly(quinine-*co*-HEA) polyplexes inside the cells. Despite the heterogeneity observed between the different particles, the radial cross sections (*SI Appendix,* Fig. S30) show that, on average, proteins are distributed throughout the polyplexes and are strongly colocalized with deintercalated quinine moieties of poly(quinine-*co*-HEA) polymer chains. For the first time, our unique combination of chemical vector design and Raman chemical imaging reveals that polyplexes are porous inside cells. Indeed, this quality enables proteins to percolate into the polyplexes, thereby unwrapping pDNA (Fig. 1*C*) for highly efficient transcription.

Conclusion

We have developed a polymeric gene delivery platform that capitalizes on the natural abundance and unique chemical and spectroscopic properties of quinine. Our synthetic approach to create QCRs uses a facile free-radical polymerization reaction that is inexpensive and scalable, making it ideal for industrial manufacture and applications. The QCR poly(quinine-*co*-HEA) acts as a robust delivery vehicle of pDNA *in vitro* and achieves efficient transgene expression across a variety of human cell types, including keratinocytes. In comparison to more conventional cationic

polymers, the excellent transfection performance of poly(quinine-*co*-HEA) can be partially attributed to two key properties. The first is that poly(quinine-*co*-HEA) packages DNA cargo through both electrostatic interactions and intercalation, which robustly stabilizes polyplex formulations during the transfection process. The second key property is that the interaction of proteins with poly(quinine-*co*-HEA) facilitates the release of pDNA cargo inside cells. These two critical attributes give poly(quinine-*co*-HEA) the proper balance between polyplex stability and cargo release to increase transgene expression efficiency for clinical gene therapy applications. The well-characterized sensitivity of quinine's vibrational modes to its local chemical environment enables us, for the first time, to exploit the chemical sensitivity encoded in Raman spectra to quantify the degree of polyplex unpackaging. In comparison to fluorescence-based methods, Raman imaging is particularly well-suited to quantify intracellular protein concentrations without the need for labeling. We employed this method to elucidate the contribution that proteins play in promoting unpackaging of a quinine-based polycationic transfection system. Our findings support long-standing speculation that intracellular proteins contribute to the release of DNA from polyplexes (**15**). The Raman chemical imaging approach applied in this work can be applied broadly to other functional materials containing quinine, and also serves as a foundation for chemical imaging of non-quinine containing materials in situ. Many functional biomaterials contain large numbers of endogenous Raman-active probes such as carbonyl, amide, nitrile, and other functional groups that, like quinine, are sensitive to their local chemical environment and can be probed via this technique. This work highlights both the potential of using QCRs as a trackable therapeutic platform and the promise of Raman-based chemical imaging methods to yield unprecedented insights into monitoring interactions of biomaterials in situ.

Materials and Methods

Detailed descriptions of the materials, methods, and additional figures are provided in the *SI Appendix*. This includes descriptions of the chemical synthesis and characterization of the polymers, assays used to study polyplex formation and stability, Raman and fluorescence microscopy experiments used to investigate transfection, and data analysis methods.

Acknowledgements

.

References

1. M. Foldvari, *et al.*, Non-viral gene therapy: Gains and challenges of non-invasive administration methods. *J. Control. Release* **240**, 165-190 (2016).
2. X. Xu, *et al.*, Delivery of CRISPR/Cas9 for therapeutic genome editing. *J. Gene Med.* **21**, e3107 (2019).
3. L. Ke, P. Cai, Y.-L. Wu, X. Chen, Polymeric nonviral gene delivery systems for cancer immunotherapy. *Adv. Ther.* **3**, 1900213 (2020).
4. R. Goswami *et al.*, Gene therapy leaves a vicious cycle. *Front. Oncol.* **9**, 297 (2019).
5. J. C. M. van der Loo, J. F. Wright, Progress and challenges in viral vector manufacturing. *Hum. Mol. Genet.* **25**, R42-R52 (2016).
6. K. Elverum, M. Whitman, Delivering cellular and gene therapies to patients: solutions for realizing the potential of the next generation of medicine. *Gene Ther.* (2019) https://doi.org/10.1038/s41434-019-0074-7.
7. C.-C. Ma, Z.-L. Wang, T. Xu, Z.-Y. He, Y.-Q. Wei, The approved gene therapy drugs worldwide: from 1998 to 2019. *Biotechnol. Adv.* **40**, 107502 (2020).
8. C. L. Hardee, L. M. Arévalo-Soliz, B. D. Hornstein, L. Zechiedrich, Advances in non-viral DNA vectors for gene therapy. *Genes (Basel)* **8**, 65 (2017).
9. M. A. Mintzer, E. E. Simanek, Nonviral vectors for gene delivery. *Chem. Rev.* **109**, 259-302 (2009).
10. P. Wu *et al.*, Non-viral gene delivery systems for tissue repair and regeneration. *J. Transl. Med.* **16**, 29 (2018).
11. W. F. Lai, W. T. Wong, Design of polymeric gene carriers for effective intracellular delivery. *Trends Biotechnol.* **36**, 713-728 (2018).
12. T. Bus, A. Traeger, U. S. Schubert, The great escape: how cationic polyplexes overcome the endosomal barrier. *J. Mater. Chem. B* **6**, 6904-6918 (2018).
13. T. Iida, T. Mori, Y. Katayama, T. Niidome, Overall interaction of cytosolic proteins with the PEI/DNA complex. *J. Control. Release* **118**, 364-369 (2007).
14. T. Okuda, T. Niidome, H. Aoyagi, Cytosolic soluble proteins induce DNA release from DNA– gene carrier complexes. *J. Control. Release* **98**, 325-332 (2004).
15. Y. Yue, C. Wu, Progress and perspectives in developing polymeric vectors for in vitro gene delivery. *Biomater. Sci.* **1**, 152-170 (2013).
16. C.-R. Luan *et al.*, Low molecular weight oligomers with aromatic backbone as efficient nonviral gene vectors. *ACS Appl. Mater. Interfaces* **8**, 10743-10751 (2016).
17. W.-J. Yi *et al.*, TACN-based oligomers with aromatic backbones for efficient nucleic acid delivery. *Chem Commun.* **50**, 6454-6457 (2014).
18. J.-H. Zhang *et al.*, Biodegradable gene carriers containing rigid aromatic linkage with enhanced DNA binding and cell uptake. *Polymers (Basel).* **10**, 1080 (2018).
19. C. J. McKinlay *et al.*, Charge-altering releasable transporters (CARTs) for the delivery and release of mRNA in living animals. *Proc. Natl. Acad. Sci. U.S.A.* **114**, E448-E456 (2017).
20. H. Luthman, G. Magnusson, High efficiency polyoma DNA transfection of chloroquine treated cells. *Nucleic Acids Res.* **11**, 1295-1308 (1983).
21. P. Erbacher, A. C. Roche, M. Monsigny, P. Midoux, Putative role of chloroquine in gene transfer into a human hepatoma cell line by DNA/lactosylated polylysine complexes. *Exp. Cell Res.* **225**, 186-194 (1996).

22. Y. Xie *et al.*, Synthesis and evaluation of chloroquine-containing DMAEMA copolymers as efficient anti-miRNA delivery vectors with improved endosomal escape and antimigratory activity in cancer cells. *Macromol. Biosci.* **18**, 1700194 (2018).

23. F. Yu *et al.*, Chloroquine-containing HPMA copolymers as polymeric inhibitors of cancer cell migration mediated by the CXCR4/SDF-1 chemokine axis. *ACS Macro Lett.* **5**, 342-345 (2016).

24. J. Cheng *et al.*, Structure-function correlation of chloroquine and analogues as transgene expression enhancers in nonviral gene delivery. *J. Med. Chem.* **49**, 6522-6531 (2006).

25. B. Zhang, Y. Zhang, S. K. Mallapragada, A. R. Clapp, Sensing polymer/DNA polyplex dissociation using quantum dot fluorophores. *ACS Nano* **5**, 129-138 (2011).

26. D. Punihaole *et al.*, New insights into quinine-DNA binding using Raman spectroscopy and molecular dynamics simulations. *J. Phys. Chem. B* **122**, 9840-9851 (2018).

27. S. N. Cohen, K. L. Yielding, Spectrophotometric studies of the interaction of chloroquine with deoxyribonucleic acid. *J. Biol. Chem.* **240**, 3123-3131 (1965).

28. W. T. Godbey, K. K. Wu, A. G. Mikos, Tracking the intracellular path of poly(ethylenimine)/DNA complexes for gene delivery. *Proc. Natl. Acad. Sci. U.S.A.* **96**, 5177-5181 (1999).

29. T. Kiang *et al.*, Formulation of chitosan-DNA nanoparticles with poly(propyl acrylic acid) enhances gene expression. *J. Biomater. Sci. Polym. Ed.* **15**, 1405-1421 (2004).

30. H. H. Chen *et al.*, Quantitative comparison of intracellular unpacking kinetics of polyplexes by a model constructed from quantum dot-FRET. *Mol. Ther.* **16**, 324-332 (2008).

31. M. L. Forrest, D. W. Pack, On the kinetics of polyplex endocytic trafficking: Implications for gene delivery vector design. *Mol. Ther.* **6**, 57-66 (2002).

32. B. G. Saar, L. R. Contreras-Rojas, X. S. Xie, R. H. Guy, Imaging drug delivery to skin with stimulated Raman scattering microscopy. *Mol. Pharm.* **8**, 969-975 (2011).

33. M. Hosokawa *et al.*, In vivo live cell imaging for the quantitative monitoring of lipids by using Raman microspectroscopy. *Anal. Chem.* **86**, 8224-8230 (2014).

34. F.-K. Lu *et al.*, Label-free DNA imaging in vivo with stimulated Raman scattering microscopy. *Proc. Natl. Acad. Sci. U.S.A.* **112**, 11624-11629 (2015).

35. F. Hu, L. Wei, C. Zheng, Y. Shen, W. Min, Live-cell vibrational imaging of choline metabolites by stimulated Raman scattering coupled with isotope-based metabolic labeling. *Analyst* **139**, 2312-2317 (2014).

36. D. Punihaole *et al.*, Glutamine and asparagine side chain hyperconjugation-induced structurally sensitive vibrations. *J. Phys. Chem. B* **119**, 13039-13051 (2015).

37. D. Punihaole, R. S. Jakubek, R. J. Workman, S. A. Asher, Interaction enthalpy of side chain and backbone amides in polyglutamine solution monomers and fibrils. *J. Phys. Chem. Lett.* **9**, 1944-1950 (2018).

38. A. V. Mikhonin, S. V. Bykov, N. S. Myshakina, S. A. Asher, Peptide secondary structure folding reaction coordinate: Correlation between UV Raman amide III frequency, Ψ Ramachandran angle, and hydrogen bonding. *J. Phys. Chem. B* **110**, 1928-1943 (2006).

39. Y. Wang, R. Purrello, S. Georgiou, T. G. Spiro, UVRR spectroscopy of the peptide bond. 2. Carbonyl H-bond effects on the ground- and excited-state structures of N-methylacetamide. *J. Am. Chem. Soc.* **113**, 6368-6377 (1991).

40. D. Punihaole *et al.*, UV resonance Raman investigation of the aqueous solvation dependence of primary amide vibrations. *J. Phys. Chem. B* **119**, 3931-3939 (2015).

41. S. C. Erfurth, E. J. Kiser, W. L. Peticolas, Determination of the backbone structure of nucleic acids and nucleic acid oligomers by laser Raman scattering. *Proc. Natl. Acad. Sci. U.S.A.* **69**, 938-941 (1972).

42. R. Alvarez, M. A. Hourdin, C. Cavé, J. D'Angelo, P. Chaminade, New polymer-supported catalysts derived from Cinchona alkaloids: Their use in the asymmetric Michael reaction. *Tetrahedron Lett.* **40**, 7091-7094 (1999).

43. J. A. Edward *et al.*, Organocatalytic synthesis of quinine-functionalized poly(carbonate)s. *Biomacromolecules* **13**, 2483-2489 (2012).

44. K. Hermann, H. Wynberg, Polymergebundene cinchonaalkaloide als katalysatoren in der Michael reaktion. *Helv. Chim. Acta* **60**, 2208-2212 (1977).

45. P. Hodge, E. Khoshdel, J. Waterhouse, Michael reactions catalysed by polymer-supported quaternary ammonium salts derived from cinchona and ephedra alkaloids. *J. Chem. Soc. Perkin Trans. 1* **1**, 2205-2209 (1983).

46. J.-H. Lee, M.-S. Yoo, S.-S. Jew, H.-G. Park, B.-S. Jeong, Polymeric chiral phase-transfer catalysts derived from cinchona alkaloids for enantioselective synthesis of α-amino acids. *Tetrahedron* **63**, 7906-7915 (2007).

47. R. Chinchilla, P. Mazón, C. Nájera, Asymmetric synthesis of α-amino acids using polymer-supported Cinchona alkaloid-derived ammonium salts as chiral phase-transfer catalysts. *Tetrahedron Asymmetry* **11**, 3277-3281 (2000).

48. A. Latorre-Sánchez, M. Johansson, Y. Zhang, M. Malkoch, J. A. Pomposo, Active quinine-based films able to release antimicrobial compounds via melt quaternization at low temperature. *J. Mater. Chem. B* **6**, 98-104 (2018).

49. B. Moon Kim, K. B. Sharpless, Heterogeneous catalytic asymmetric dihydroxylation: Use of a polymer-bound alkaloid *Tetrahedron Lett.* **31**, 3003-3006 (1990).

50. I. Minoru, H. Jun, Y. Yukio, O. Jun'ichi, Asymmetric induction in the base-catalyzed reactions using polymer-supported quinines with spacer groups. *Bull. Chem. Soc. Jpn* **60**, 4121-4126 (1987).

51. N. Kobayashi, K. Iwai, Functional polymers. 1. Poly(cinchona alkaloid-co-acrylonitrile)s. New polymer catalysts for asymmetric synthesis. *J. Am. Chem. Soc.* **100**, 7071-7072 (1978).

52. S. M.-A. Borchan, I. V. Zadneprovskaya, T. M. Babayev, U. N. Musayev, Copolymerization of N-vinylpyrrolidone with quinine. *Polym. Sci. U.S.S.R.* **29**, 43-49 (1987).

53. G. A. Mortimer, L. C. Arnold, Free-radical polymerization of olefins. *J. Polym. Sci. Part A Gen. Pap.* **2**, 4247-4253 (1964).

54. G. Odian, "Radical chain polymerization" in Principles of Polymerization, 198-349 (2004).

55. Y. Liu, T. M. Reineke, Poly(glycoamidoamine)s for gene delivery. Structural effects on cellular internalization, buffering capacity, and gene expression. *Bioconj. Chem.* **18**, 19-30 (2007).

56. Y. Liu, L. Wenning, M. Lynch, T. M. Reineke, New poly(D-glucaramidoamine)s induce DNA nanoparticle formation and efficient gene delivery into mammalian cells. *J. Am. Chem. Soc.* **126**, 7422-7423 (2004).

57. D. Sprouse, T. M. Reineke, Investigating the effects of block versus statistical glycopolycations containing primary and tertiary amines for plasmid DNA delivery. *Biomacromolecules* **15**, 2616-2628 (2014).

58. Y. Liu, T. M. Reineke, Poly(glycoamidoamine)s for gene delivery: Stability of polyplexes and efficacy with cardiomyoblast cells. *Bioconj. Chem.* **17**, 101-108 (2006).

59. S. Srinivasachari, Y. Liu, L. E. Prevette, T. M. Reineke, Effects of trehalose click polymer length on pDNA complex stability and delivery efficacy. *Biomaterials* **28**, 2885-98 (2007).
60. D. Goula *et al.*, Size, diffusibility and transfection performance of linear PEI/DNA complexes in the mouse central nervous system. *Gene Ther.* **5**, 712-717 (1998).
61. R. S. Burke, S. H. Pun, Extracellular barriers to in vivo PEI and PEGylated PEI polyplex-mediated gene delivery to the liver. *Bioconj. Chem.* **19**, 693-704 (2008).
62. D. Pezzoli, E. Giupponi, D. Mantovani, G. Candiani, Size matters for in vitro gene delivery: Investigating the relationships among complexation protocol, transfection medium, size and sedimentation. *Sci. Rep.* **7**, 44134 (2017).
63. P. Agrawal *et al.*, Fast, efficient, and gentle transfection of human adherent cells in suspension. *ACS Appl. Mater. Interfaces* **8**, 8870-8874 (2016).
64. D. Luo, W. M. Saltzman, Enhancement of transfection by physical concentration of DNA at the cell surface. *Nat. Biotechnol.* **18**, 893-895 (2000).
65. Z. Tan *et al.*, Polycation architecture and assembly direct successful gene delivery: Micelleplexes outperform polyplexes via optimal DNA packaging. *J. Am. Chem. Soc.* **141**, 15804-15817 (2019).
66. K. von Gersdorff *et al.*, The internalization route resulting in successful gene expression depends on both cell line and polyethylenimine polyplex type. *Mol. Ther.* **14**, 745-753 (2006).
67. J. Rejman, V. Oberle, I. S. Zuhorn, D. Hoekstra, Size-dependent internalization of particles via the pathways of clathrin- and caveolae-mediated endocytosis. *Biochem. J.* **377**, 159-169 (2004).
68. F. Mavilio *et al.*, Correction of junctional epidermolysis bullosa by transplantation of genetically modified epidermal stem cells. *Nat. Med.* **12**, 1397-1402 (2006).
69. J. W. Bauer *et al.*, Closure of a large chronic wound through transplantation of gene-corrected epidermal stem cells. *J. Invest. Dermatol.* **137**, 778-781 (2017).
70. T. Hirsch *et al.*, Regeneration of the entire human epidermis using transgenic stem cells. *Nature* **551**, 327-332 (2017).
71. A. F. Deyrieux, V. G. Wilson, In vitro culture conditions to study keratinocyte differentiation using the HaCaT cell line. *Cytotechnology* **54**, 77-83 (2007).
72. S. Dickens *et al.*, Nonviral Transfection Strategies for Keratinocytes, Fibroblasts, and Endothelial Progenitor Cells for Ex Vivo Gene Transfer to Skin Wounds. *Tissue Engineering Part C: Methods* **16**, 1601-1608 (2010).
73. X. Liang *et al.*, Rapid and highly efficient mammalian cell engineering via Cas9 protein transfection. *J. Biotechnol.* **208**, 44-53 (2015).

74. C. Zhao *et al.*, Probing structure-antifouling activity relationships of polyacrylamides and polyacrylates. *Biomaterials* **34**, 4714-4724 (2013).
75. M. Zolk *et al.*, Solvation of oligo(ethylene glycol)-terminated self-assembled monolayers studied by vibrational sum frequency spectroscopy. *Langmuir* **16**, 5849-5852 (2000).
76. J. Zheng, L. Li, S. Chen, S. Jiang, Molecular simulation study of water interactions with oligo (ethylene glycol)-terminated alkanethiol self-assembled monolayers. *Langmuir* **20**, 8931-8938 (2004).